CAAP Annual Report

Date of Report: *09/30/2023*

Prepared for: *U.S. DOT Pipeline and Hazardous Materials Safety Administration*

Annual Period: **From** *(10, 01, 2022)* **to** *(09, 30, 2023)*

Contract Number: *693JK3215002CAAP*

Project Title: *Easy Deployed Distributed Acoustic Sensing System for Remotely Assessing Potential and Existing Risks to Pipeline Integrity*

Prepared by: *Yilin Fan, Ge Jin, Ali Tura, Jennifer Miskimins*

Contact Info.: *yilinfan@mines.edu, 303-273-3749*

Table of Contents

Section A: Business and Activities

(a) Contract Activities

- Contract Modifications:

  During the past reporting period, the budget narrative has been updated to consider the changing situations since the initial submission of the proposal and enable more flexibility that aids in the smooth progress of the project activities. It has been approved by the agreement officer (AO).

- Educational Activities:

  - Student mentoring:

    Two Ph.D. students are fully engaged in this project since 2021S. They are:

    1. Ana Garcia-Ceballos, Ph.D. student in Geophysics
    2. Mouna-Keltoum Benabid, Ph.D. student in Petroleum Engineering

    In addition, various students have been involved in this project and offered temporary support to this project as needed. The students who have made substantial contributions to this project in this reporting year include:

    1. Victor Fakeye, Ph.D. student in Geophysics at Colorado School of Mines, supported this project on data processing.
    2. Peyton Baumgartner, Undergraduate student in Petroleum Engineering at Colorado School of Mines, supported this project on the experimental program.
    3. Raad Al-saifi, Undergraduate student in Petroleum Engineering at Colorado School of Mines, supported this project in the experimental program.
    4. Binghao Li, Undergraduate student in Geophysics at University of Science and Technology of China, did an internship at Colorado School of Mines and supported this project on data processing and in the experimental program.

  - Student internship:

    In 2023 Summer, Ana Garcia-Ceballos did an internship at BP, and Mouna-Keltoum Benabid did an internship at Chevron.

  - Educational activities:

    During the past period, we educated the students who have been participating in this project on relevant pipeline integrity problems and diagnosis technologies.

  - Career employed:

    None.

- Others:

  None.

- Dissemination of Project Outcomes:

  None.

- Citations of The Publications:

  None.

- Others:

  None.

(b) Financial Summary

This financial summary was prepared on 9/29/23. Please note that the actual amount in the final annual financial report might be slightly different from the numbers shown below, since some of the expenses occurring in late the year may not be shown in the university's financial system that we use for managing the funds and expenses by the time the report is submitted. Normally, it takes several days for an expense to be shown in the system after its occurrence.

- Federal Cost Activities:

  - PI/Co-PIs/students involvement:

    The table below summaries the expenses for PI/Co-PIs/Students during the past year:

Items\Budget and Expenses		Budget for Year 2	Expenses
1	Faculty Salaries, Wages, and Fringe Benefits	$28,510	$28,191
2	Student Salaries	$65,920	$58,535
3	Graduate Student Tuition	$46,260	$47,364

  - Materials purchased/travel/contractual (consultants/subcontractors):

Items\Budget and Expenses		Budget for Year 2	Expenses
1	Experimental Expenses (experimental work supplies, services, maintenance, cables, air compressor operations, etc.)	$27,000	$21,255
2	Travel	$3,000	$1,750

The indirect cost in the past year is around $55,997.

The total expense is around $213,092.

The total budget up to 9/30/2023 is $260,512, including the budget for the second year $235,392, and the amount left from the previous year $25,119.

- Cost Share Activities:
    - Cost share contribution: The cost share is the AY efforts of the PI and co-PIs, that makes up 20% of the total expenses.

(c) Project Schedule Update

- Project Schedule:

Since the 1st annual report, the project schedule has been updated slightly due to the challenges faced during the past period.

In summary, Tasks#1 and #5 have been completed as scheduled. Task#2 is slightly ahead of schedule. Tasks#3, 4, and 6 are slightly behind schedule. However, since the test sections are almost ready, we are optimistic that these tasks can be completed on time. The major factors that caused the delay are that the two Ph.D. students assigned to this project did an internship in 2023 summer and one of the Ph.D. students is still suffering from her ankle injury that prohibits her from doing experiments. We fortunately hired some students temporarily during the summer time. After several intense training sessions, we have made noticeable progress during this difficult time. The other factors are that the other Ph.D. student was back to campus late due to some personal issue while the other UG students are only available on Fridays to run experiments due to the class and Edgar Mine's working schedule, and Edgar Mine's air compressor was shut-in for around half a month due to the conflicts with other events. Because of these factors, we update the project schedule, which is shown in the table below. However, since the 1-m test sections for Tasks#3, #4, and #6 are almost ready (see details in the technical section), we anticipate that these tasks will be continued soon in the next quarter.

Tasks	Year 1				Year 2				Year 3			
	Q1	Q2	Q3	Q4	Q1	Q2	Q3	Q4	Q1	Q2	Q3	Q4
	2021	2022			2023				2024			
	O-D	J-M	A-J	J-S	O-D	J-M	A-J	J-S	O-D	J-M	A-J	J-S
Task#1. Detection of Liquid Accumulation at Pipeline Lower Spots												
1.1 Facility modification and preparation												
1.2 Flow loop test without liquid accumulation												
1.3 Flow loop tests with liquid accumulation												
Task#2. Detection of Dynamic Intermittent (Slug) Structure												
2.1 Flow loop tests with Interminttent Structure												
Task#3. Detection of Corroded Spots on Pipeline Interior												
3.1 Facility modification and preparation												
3.2 Lab tests of corrosion using speciman to determine acid type, concentration, and corrosion rate												
3.3 Flow loop test in buried pipe												
3.4 Flow loop test in unburied pipe												
3.5 Flow loop test in densely supported pipe												
3.6 Flow loop test in sparsely supported pipe												
Task#4. Detection of Dent/Deformation on Pipeline												
4.1 Flow loop test in buried pipe												
4.2 Flow loop test in sparsely supported pipe												
Task#5. Detection of Infrastructure Damage												
5.1 Flow loop test in densely supported pipe												
5.2 Flow loop test in sparsely supported pipe												
Task#6. Detection of Leakage												
6.1 Flow loop test in buried pipe												
6.2 Flow loop test in sparsely supported pipe												

densely or sparsely supported unburied buried

- Corrective Actions:

  None.

(d) Status Update of the 4th or 8th Quarter Technical Activities

- Task 1: Detection of Liquid Accumulation at Pipeline Lower Spots

  This task has been completed by the 6th quarter.

- Task 2: Detection of Dynamic Intermittent (Slug) Structure

  During the 8th quarter, we revamped the multiphase flow facility, and finished the experiments for one constant water flow rate at 0.005m/s at various gas flow rates from 18 to 2 m/s. We performed and explored different data processing approaches. The data shows that DAS captures very well the flow pattern transition and the slug flow structures. The data also shows a good correlation with the measurement from a point pressure sensor. The sensitivity of various cable types was evaluated by comparing a single channel near each pressure sensor for each cable type. The flat cables exhibited the highest sensitivity, followed by thin, straight, helical, and thick cables. Details can be found in Section 3.2 or the 8th quarterly report.

- Task 3: Detection of Corroded Spots on Pipeline Interior Surface

  In the 8th quarter, we prepared a 1-m test section with severe internal corrosion that resulted in a small leakage (2mm) at the pipe bottom. We are in preparation for another 1-m test section with a target of 5.5 corrosion depth (pipe wall thickness is 6.019mm), to simulate the condition of severe internal corrosion but without leakage. The flow tests will be conducted in the next quarter.

- Task 4: Detection of Dent/Deformation on Pipeline

  In the 8th quarter, we worked with EMI (the Excavation Engineering and Earth Mechanics Institute) at the Colorado School of Mines on the fabrication of dents in the 1-m test section. We have successfully prepared two deformed pipes with different dent sizes. The pipe that exhibits a substantial deformation represents a significant structural compromise, while the other that showcases a smaller dent simulates a less severe scenario. The pictures can be found in Section 3.5 or the 8th quarterly report. We intend to test these two differently deformed pipes in the flow loop during the upcoming reporting period.

- Task 5: Detection of Infrastructure Damage

  This task has been finished by the 7th quarter.

- Task 6: Detection of Leakage

  In the 8th quarter, we conducted the leakage experiments and tested four different leakage sizes (¼", ½", ¾", and 1") and 3 orientations (bottom, side, and top) at 5 different gas flow rates (2, 6, 10, 14, 18 m/s). We have spent lots of effort exploring different data processing algorithms to better understand the DAS signal and its relationship to the flowing conditions. In summary, the black and flat cables successfully capture the leakages at the pipe bottom. The vibration anomaly appears to diminish with decreasing hole size and is entirely absent in the control tests with no leakage. The thick cable is less sensitive and can only detect leakage larger than ½" for a 10 m/s gas flow rate. Leakage detection sensitivity is also influenced by the gas flow rate within the pipe. Details can be found in Section 3.6 or the 8th quarterly report. Our findings suggest that black and flat cables offer the most reliable leakage detection results to date. Their lighter and more flexible structures likely render them more sensitive to fluid movements within the pipe. We performed the same analysis for the side and top leakages, however, since the control tests were performed on a different day, the signals were not as clear as the ones for the bottom leakage tests. We plan to explore the causes and repeat the tests in the next quarter.

Section B: Detailed Technical Results in the Report Period

1. Background and Objectives in the 2nd Annual Report Period

1.1. Background

There are more than 220,000 miles of hazardous liquid or carbon dioxide pipeline system and 320,000 natural gas transmission and gathering pipelines traverse the United States as of 2019 according to the latest annual report from U.S. Department of Transportation Pipeline and Hazardous Materials Safety Administration. Reliable assessment of pipeline integrity is of greatest importance to the environment, economy, and society. Pipeline failure can be induced by various sources, such as internal or external corrosion (including microbiologically influenced corrosion), stress corrosion cracking, material/weld failure, excavation damage, incorrect operations, and natural force damages (i.e., seismic events, flooding, lightning, etc.).

Some widely used and/or studied pipeline integrity assessment techniques include in-line inspection (ILI) tools, such as "smart pigs" and robots, and hydrostatic pressure tests. ILI tools travel through the pipe and measure and record irregularities that may represent corrosion, cracks, laminations, deformations (dents, gouges, etc.), or other defects [1]. However, these tools are not always applicable to pipelines. They also require pipeline operators to periodically conduct investigations, which consumes an enormous amount of time and affects oil and gas production [2]. Hydrostatic pressure tests can pose additional risks to the pipeline integrity due to excessive pressure cyclic that can lead to fast growing of cracks and rupture.

Distributed Fiber-Optic Sensing (DFOS) is a recent trending technology for remote pipeline integrity monitoring. By connecting the instrument to one end of a regular telecommunication fiber, DFOS systems can take distributed measurements along the fiber with high spatial and temporal resolution. Modern system development allows a single instrument to measure more than 50-km of fiber simultaneously [3], which is highly cost-effective for pipeline monitoring purposes. DFOS systems include Distributed Acoustic Sensing (DAS), Distributed Temperature Sensing (DTS), and Distributed Strain Sensing (DSS).

Compared with other technologies such as ILI and pressure tests, DFOS has established many advantages in several aspects. First, it can provide continuous monitoring of pipeline operating conditions and remote detection of leaks [4] without disturbing production and operation, while most other technologies provide one-time investigation and require operators to conduct assessments periodically. The continuous monitoring also enables the operators to track the changes in operation conditions (such as pressure cyclic events that can lead to a faster cracking) and potentially the change/growth of existing threats with time, which can significantly promote the fundamental understanding of crack growth rate with operating conditions and/or environment. Second, DFOS provides real-time monitoring and can provide quick responses in remote areas without waiting for days after the leaks dramatically occur, such that the operators

can take immediate actions to avoid catastrophic damage due to late responses. It can also detect and localize any anomaly due to natural forces and human intrusion, such that the operators will be more cautious about potential threats in that area.

Many works have been done to investigate the feasibility of using DFOS systems for pipeline monitoring applications. Early studies demonstrated that by placing the sensing fiber cable underneath or close to the pipeline, DTS can detect and locate anomalous temperature variations induced by fluid or gas leakage [5–7]. If the fiber is mechanically coupled to the pipeline using glue, tape, or clamp, bending and deformation of the pipeline infrastructure can also be detected [2,8]. One of the previous studies [9] showcased a long-term field pipeline monitoring program using DTS and DSS where leakage, landslide, and surface subsidence events were successfully detected and monitored.

Besides DTS and DSS, DAS is capable of monitoring vibrations of and near the pipelines, with high temporal and spatial resolutions. By sending a coherent laser pulse into the fiber, DAS interrogator measures the phase changes of the back-scattered laser energy, which can then be converted to distributed strain rate measurements. A typical DAS instrument can measure more than 6000 locations (channels) simultaneously, with a temporal sampling rate of more than 10 kHz (fiber length dependent), making it an ideal tool to monitor pipeline vibrations remotely and in real-time.

The usage of DAS for pipeline monitoring has also been investigated in recent years. Tejedor et al. [10] demonstrate that using DAS signal detect pipeline intrusion events. Stajanca et al. [11] show that DAS signal is also sensitive to leakage-related vibrations. However, the study was not able to separate the pipe infrastructure vibrations from the vibrations induced by leakage, especially in the high pressure, high flow rate examples. A more recent study characterized leakage noise for buried gas pipelines, measured using different DAS cable designs [4]. The experiment was set up to minimize the pipeline vibrations so the recorded data were dominated by leakage signals.

Most of the previous studies focus on leakage or intrusion-induced vibrations, and treat pipeline vibration induced by flow as unwanted and environmental “noise”. However, flow-induced vibrations contain critical information for pipeline health and risk assessment. Large pipeline vibrations may be related to improper pipeline installation, damaged supporting infrastructure, or unwanted slug flow within the pipeline. Prolonged vibrations may also compromise the life span of the infrastructure, and increase the risk of external corrosion and damage at the joint and supporting/contact points.

The flow-induced pipeline vibration has been intensively studied in the past several decades [12–15]. It is not the intention of this proposal to repeat or extend previous research to understand the fundamental physics of vibrations. Rather, we focus on understanding the flow-induced vibrations that are associated with potential risks for pipeline integrity, and how these vibrations interact with sensing fiber cables.

Sensing fiber installation along the pipeline significantly affects the cost and effectiveness of the remote sensing system. Wrapping fiber around the pipe can provide the best spatial resolution and sensitivity to the pipe vibration, but significantly increases

the installation cost and shortens the sensing range. Clamping or taping a straight fiber outside the pipe are more practical options, but can still be expensive or impossible for buried pipelines. Deploying a sensing cable inside the pipeline can be much cheaper and easier compared to external cable deployment, as the cable can either be pumped down or dragged along by a tractor device. However, cable inside the pipeline can be directly affected by the flow, which imposes challenges on sensing the pipeline vibration directly. Meanwhile, different cable structural designs also affect the sensing results.

1.2. Objectives in the 2nd Annual Report Period

In this project, we plan to solve and answer several fundamental but practical questions for using DAS to assess pipeline integrity risks, which include:

- The feasibility of using DAS to identify vibrations that are associated with pipeline integrity risks, which include liquid accumulation at lower spots, slug flow, internal corrosion, dent, damaged infrastructure, and leakage.

- The effectiveness of sensing the aforementioned vibrations using different sensing cable deployment methods, especially for cables inside the pipeline.

2. Experimental Program in the 2nd Annual Report Period

2.1. Experimental Design

To achieve the research goal, we perform the experimental study at Edgar Mine, an experimental mine of Colorado School of Mines (CSM) located approximately 20 miles west of Denver. The location and picture of the experimental facility are shown in Figure 1. The flow loop is inside the tunnel, which has a very quiet environment that eliminates measurement uncertainties. The mine is relatively dry and has a constant year-round temperature of 54°F. The mine is well-equipped with utility systems that allow the operation of equipment for maintenance and experimentation.

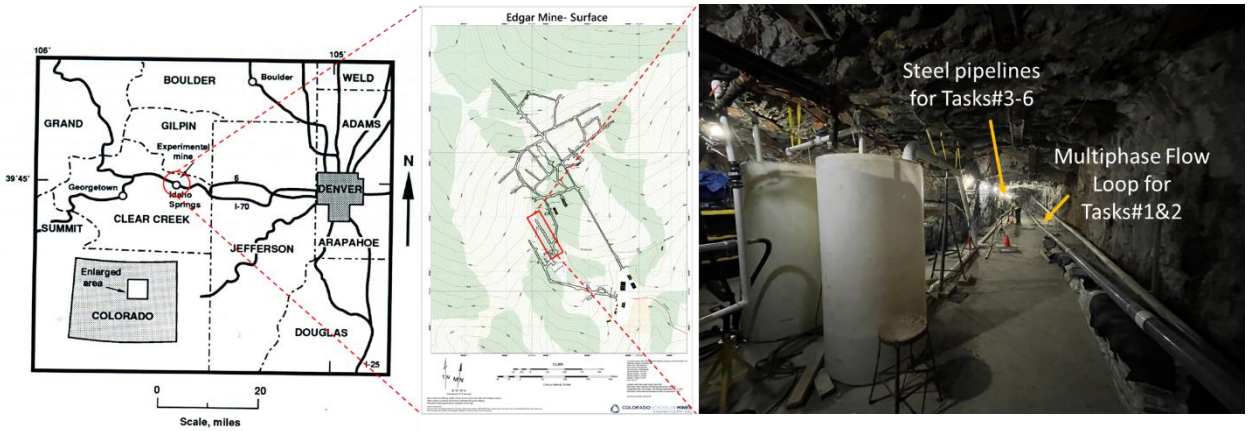

Figure 1. Testing facility for this project at Edgar Mine.

Tasks#1 and #2

The experimental design for Task #1, focused on the Detection of Liquid Accumulation at Pipeline Lower Spots, and Task #2, aimed at the Detection of Dynamic Intermittent (Slug) Structures, utilizes a transparent PVC pipeline flow loop. This configuration enables the direct observation of flow behavior for subsequent comparison with recorded DAS data.

To create a low spot for the accumulation of water, a custom PVC pipe was fabricated with specific inclinations. The test section has a lower spot, 43 ft from the beginning of the flow loop, followed by a 2-degree upward inclined pipe. The total length of the experimental side of the flow loop, comprising the clear PVC section, extends to 150 ft.

An external single-mode jacket cable was helically wrapped around the exterior of the clear PVC pipes. For every 10 ft of pipe, 100 ft of cable was employed, resulting in a spacing of 3 cm between each cable wrap. Tension and duct tape were utilized to secure the cable in place. Three internal cables of varying thicknesses (thin, thick, and flat) were deployed within the PVC pipes, where they were positioned freely. These internal cables exit the pipe through custom-designed seals located at opposing ends of the clear PVC section. Figure 2 shows the schematic of the multiphase flow test section, depicting the connection of the fiber optic cables.

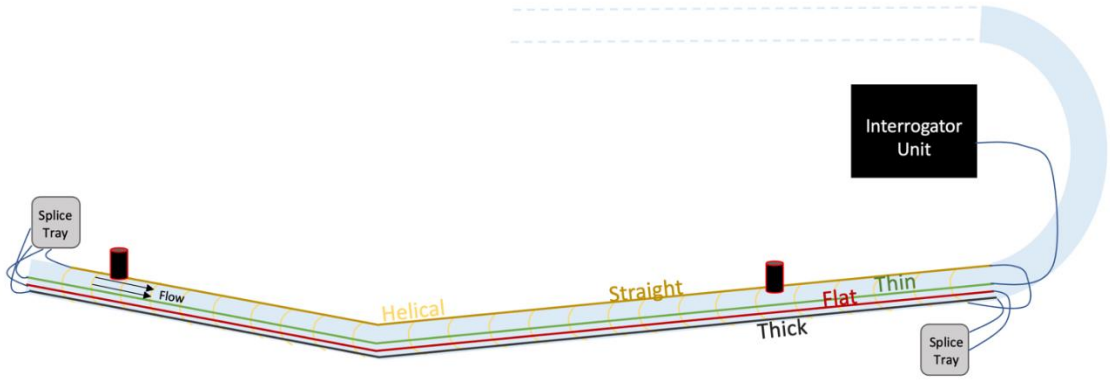

Figure 2. Schematic of Task#1 and #2 layout, depicting the interrogator unit spliced to a sequence of cables – thin, flat, thick, straight, and helical. Two pressure sensors, shown as black cylinders in the schematic, are positioned both uphill and downhill along the experimental section of the flow loop.

For Task#2, two additional pressure sensors were installed. One sensor was placed at the inlet, downstream and downhill from the start, while the second sensor was positioned in the middle of the uphill section. Both pressure sensors were interfaced with a LabView Data Acquisition system, as were the control valves responsible for regulating the air and water inlets. Furthermore, modifications were made at the outlet of the multiphase flow loop into the water tank. This involved replacing PVC pipes with inclined configurations to minimize turbulence and reduce noise associated with water discharge into the tank. Figure 3 shows a picture of the multiphase flow facility, as well as some

pictures of the slug flow from Task#2.

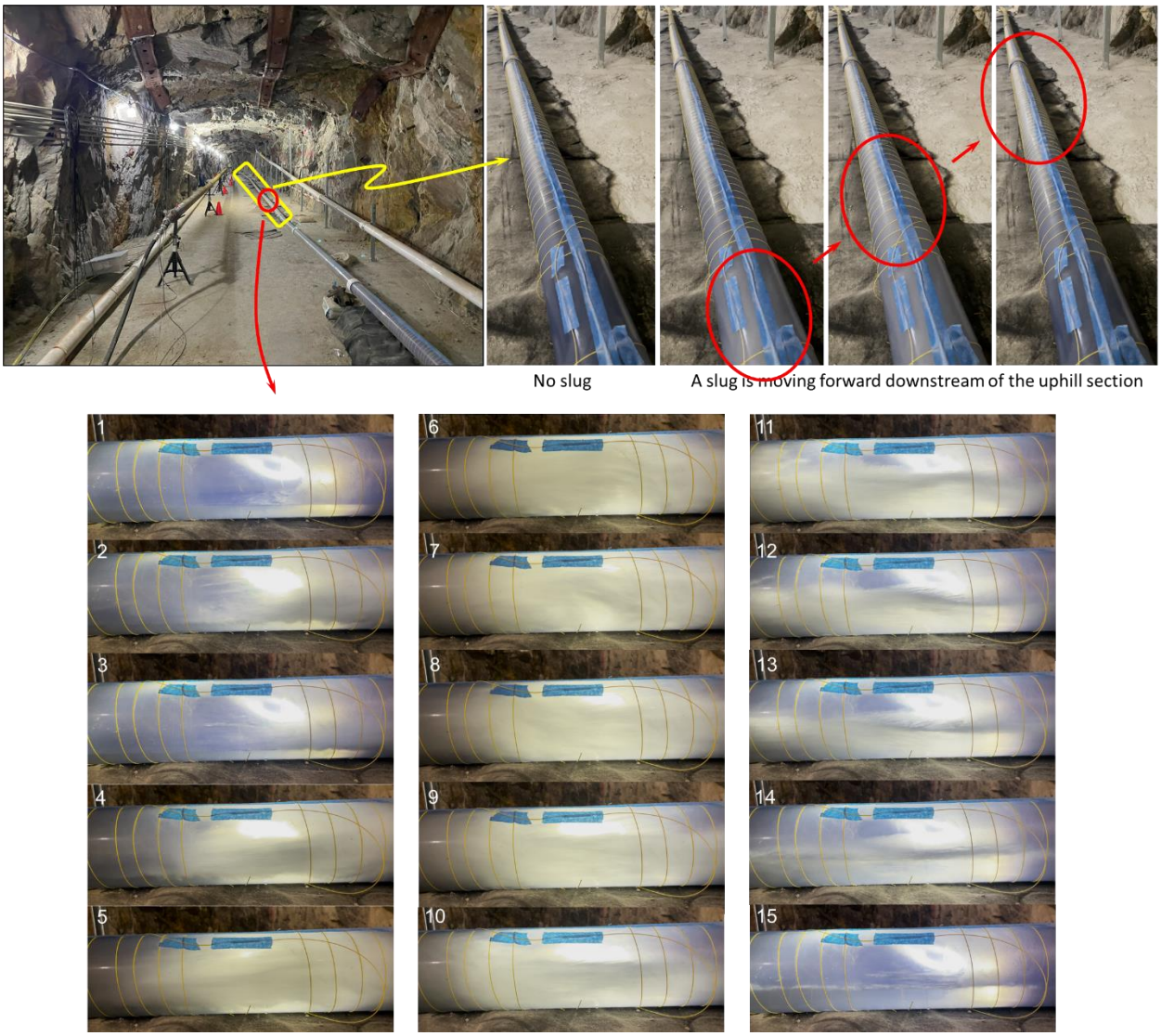

Figure 3. Pictures of the multiphase flow loop (top left) and a slug (top right and bottom) from Task#2.

Tasks#3 to #6

Tasks #3-6 are all carried out in a steel pipeline. During this reporting period, we finalized the construction and modification of the pipeline utilizing carbon steel seamless pipes (API 5L, schedule 40, NPS 4-in, grade X65). The pipeline consists of four 5-m sections, with a 1-m pipe segment positioned in the center (Figure 4).

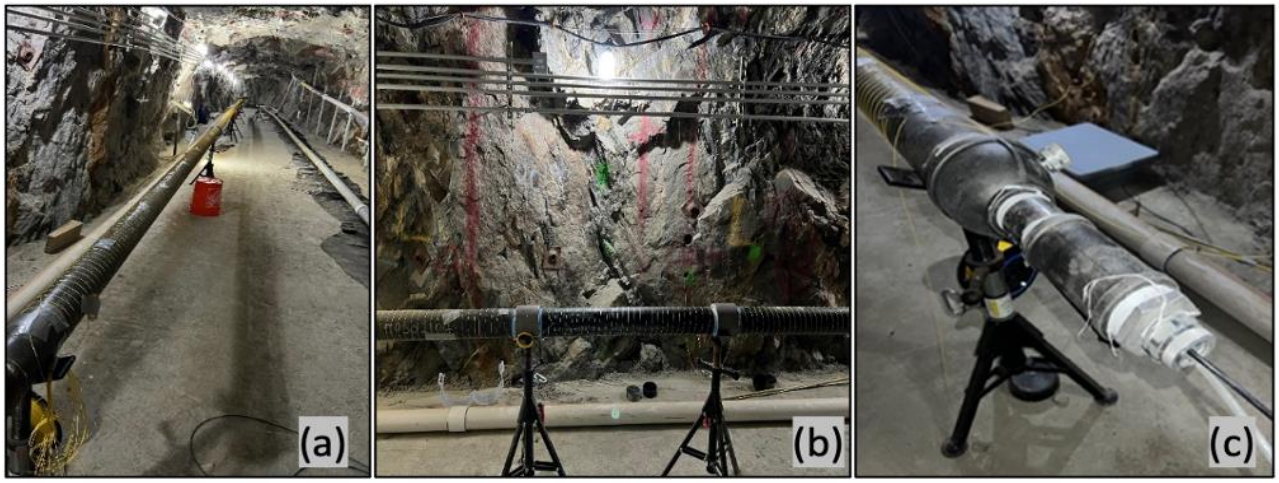

Figure 4. (a) Photograph of the optical fiber deployed along the steel pipeline; (b) Photograph of the 1-m section in the middle of the steel pipeline; (c) Photograph of the rubber-sealed inlets used to deploy the internal cables.

The lessons learned from Tasks #1 & 2's cable deployment have demonstrated that the thin cable from Neubrex Technologies company is very delicate for a field setting, and can barely survive in harsh environments. Additionally, from preliminary data analysis, the thin cable is the least sensitive to flow. As a result, the cables implemented in Tasks #3-6 have been reevaluated. Instead of using thin cable that has been shown to be not practical for a harsh field setting, a ground-tactical cable from OCC (referred to as black cable in this project) that is more robust for harsh environments is deployed. In total, the steel pipeline incorporates five distinct fiber optic cables. These fiber cables are sequentially spliced in the following order: starting with the straight external yellow cable connected to the black cable, followed by the flat cable, then the thick cable, and finally joined to the external helically wrapped cable (Figure 5). The yellow helically wrapped fiber is initially applied along the 10-m sections at both the beginning and end of the steel pipeline. However, the 1-m test section in the middle was intentionally left unwrapped until the very end. This simplifies the process of replacing the 1-meter section according to the task studied. The five cables are connected to the Terra15 interrogator that enables DAS data acquisition.

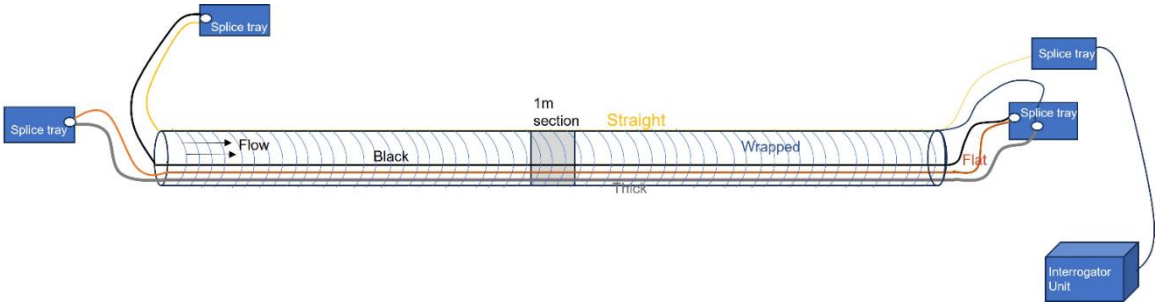

Figure 5. A schematic diagram showing the order of cable connection on the steel pipeline. The two black arrows indicate the direction of flow. Order of looped cable: Straight – Black – Flat – Thick – Wrapped.

Two rubber-sealed inlets are used to introduce the internal cables (thick, black, and flat), as shown in Figure 4c. The rubber-sealed fittings are assembled in a flexible manner to allow the easy movement of the internal cables, and the change of the 1-m test section situated in the middle of the steel pipeline with the least re-splicing needed. The entire steel pipeline is connected to the main air supply from the Mine air compressor using a flexible hydraulic hose, and is supported with tripods, as shown in Figure 4. The number of tripods in place is changed accordingly to test the different configurations proposed for the project densely and sparsely supported pipelines.

The core experimental framework remains consistent across Tasks #3-6, primarily involving the running of single-phase air at varying velocities, approximately 2 m/s, 6 m/s, 10 m/s, 14 m/s, and 18 m/s. The key variation is the customization of the central 1-meter pipe to correspond with the specific studied task, as follows:

- Task#3: In this task, the central pipe incorporates a 1-m test section with varying levels of corrosion, simulating three scenarios: one representing moderate corrosion with a depth of 3 mm, the second referring to severe corrosion with a depth of 5.5 mm approximately without penetration, and the third referring to severe corrosion with minor penetration. Further details on the laboratory experiments to induce corrosion on the internal pipe surfaces and achieve the desired corrosion depths will be provided in the upcoming Test Procedure section.

- Task#4: This task entails the replacement of the 1-m test section with a deformed pipe to replicate dented pipelines commonly encountered in field conditions. We plan to test two different dent sizes, which will be shown in Section 3.4.

- Task#5: In this task, we investigate the infrastructure damage detection, the central 1-m section remains intact, with no corrosion, deformation, or leakage. The only modification involves varying the number of tripods supporting the entire pipeline. In the base case for the sparsely supported pipeline, 5 supports are evenly distributed along the 21-m steel pipeline. One support, the second from the inlet, was removed to simulate the scenario of support damage, resulting in a total of 4 supports for the damaged support condition. For the densely supported pipeline, 6 supports were used in the base case, and the second one from the inlet was removed to simulate the support damage.

  Task#6: It involves a 1-m test section with 1" holes at three different positions (top, side, and bottom), enabling the simulation of leakage at various orientations. A picture of the facility is shown in Figure 6a. Combined with reducers with three different sizes (Figure 6d), we can simulate four leakage sizes, namely ¼", ½", ¾", and 1". Five gas flow rates, namely 2, 6, 10, 14, 18 m/s, will be tested. Additionally, a pressure sensor is incorporated to record central pipe pressure during experiments. A removable cap is installed at the pipe outlet to increase the pressure differential between the pipe and atmospheric conditions at the leakage points, enhancing data quality and DAS detectability.

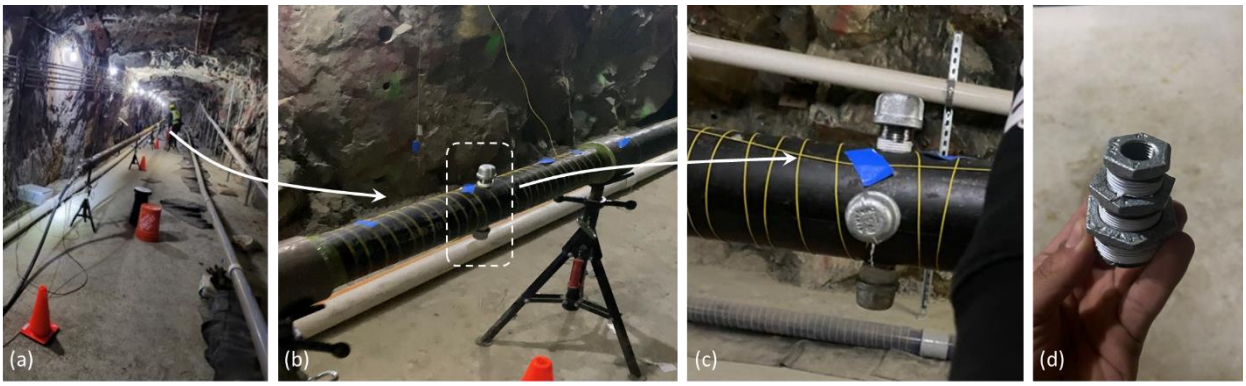

Figure 6. (a) A picture of the facility; (b) 1-m test section for leakage detection; (c) holes with caps on the 1-m test section; (d) reducers for hole size control

2.2. Test Procedure

- Laboratory Testing:

For Task#1, the test procedures of the experimental studies involved varying stagnant accumulated water volumes, specifically 4L, 10L, and 20L, at velocities of approximately 2 m/s, 4 m/s, and 6 m/s. Adjustments to the air flow valve were made to achieve the desired velocities mentioned earlier. These velocities were maintained for a minimum of 10 minutes to ensure that the flow reached a fully developed state.

For Task #2, which focused on the Detection of Dynamic Intermittent (Slug) Structures, a combination of air and water was introduced into the PVC pipe flow loop. The water valve was kept constant to maintain a constant flow rate. Concurrently, adjustments to the air valve were made to attain various target velocities: 18 m/s, 16 m/s, 14 m/s, 12 m/s, 10 m/s, 8 m/s, 6 m/s, 4 m/s, and 2 m/s. Additionally, single-phase experiments were conducted at the same velocities as the multiphase experiments to establish a baseline for comparison.

For Task#3, the same procedures and methods outlined in the 1st year annual report were employed to induce corrosion in the 1-m test sections. This includes: 1) 400 ml of hydrochloric acid (12M) is introduced into the 1-m pipe section to initiate corrosion at the 6 O'clock position. The acid is replaced every 24 hours. 2) A general corroded depth is generated, and mechanical grinding is applied to create surface scratches, increasing the pipe wall's roughness. 3) For the purpose of accelerating the corrosion rate, a heating system is utilized to increase the temperature of the acid within the pipe. An optimal temperature of 65°C was identified and maintained during the corrosion lab experiments. This temperature enhancement played a crucial role in attaining the targeted corrosion rate. Figure 7 shows the 1-m test section during an ongoing experiment creating the corroded internal surface. We successfully corroded two 1-m pipes, with one simulating a scenario of moderate wall corrosion, featuring a depth of 3 mm, and the other representing a severe corrosion case with a depth of approximately 5.8 mm and a small penetration (see Section 3.6).

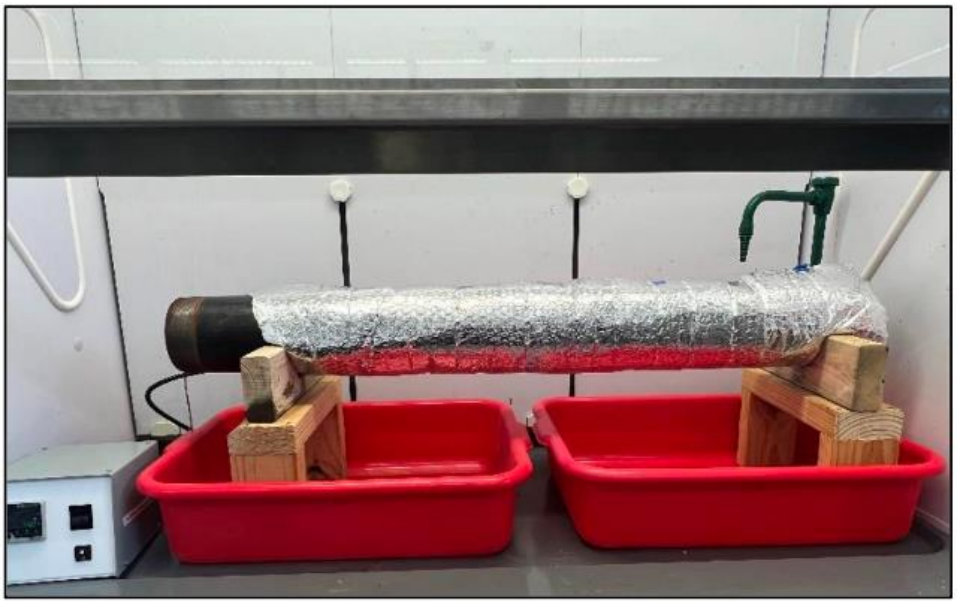

Figure 7. Photograph of the 1-m steel pipe during an ongoing lab corrosion preparation

- Field Testing:

  None.

3. Results and Discussions

3.1. Task#1: Detection of Liquid Accumulation at Pipeline Lower Spots

The results obtained from experiments involving water volumes of 4L, 10L, and 20L at velocities of 2 m/s, 4 m/s, and 6 m/s, as recorded by DAS data, reveal promising capabilities in the detection of liquid accumulation within pipeline low points. Figure 8 shows the processed DAS data recorded with around 4 m/s gas velocity with the three different water volumes. A clear low-frequency vibration can be observed by the flat cable near the V section, which is associated with wavy liquid surface and water-cable interaction.

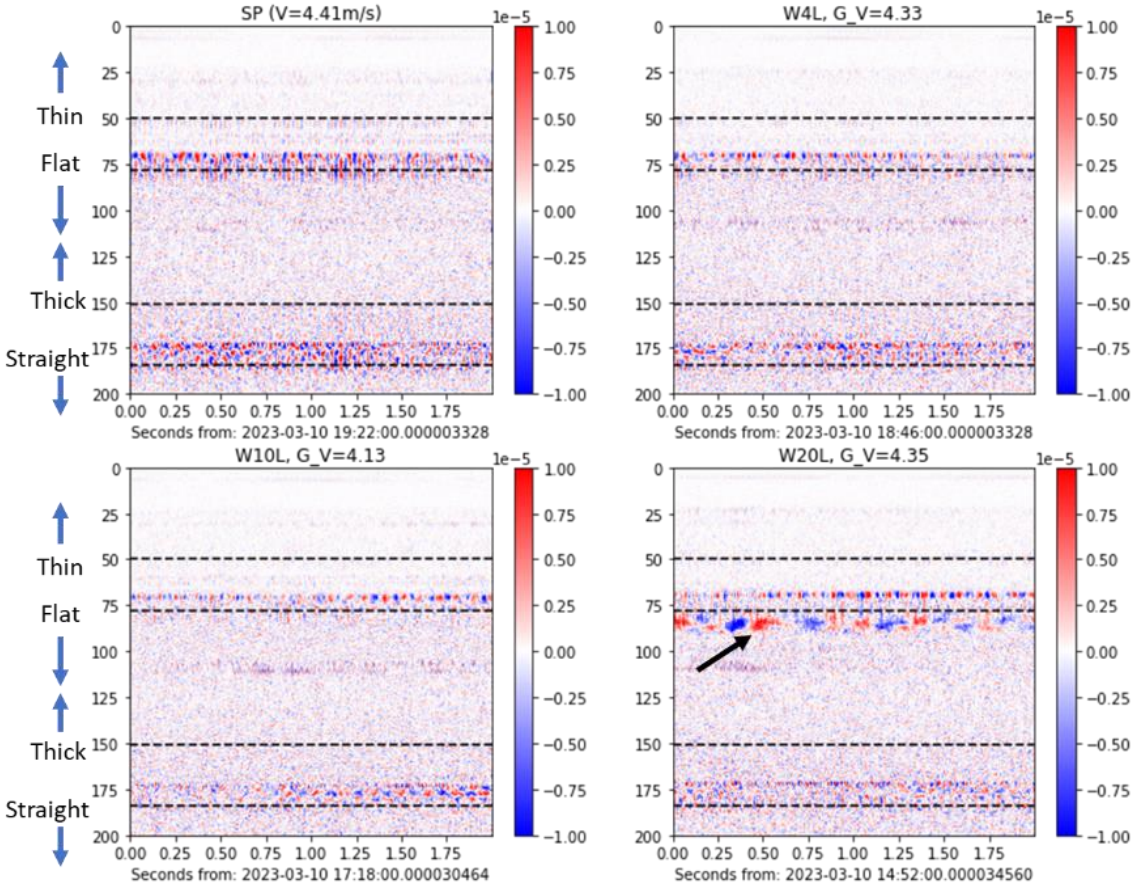

Figure 8. Waterfall plots for DAS raw data all observed at around 4 m/s gas velocity with different volumes of water accumulated at the V-section. The vertical axis is distance along the fiber in meter, and horizontal axis is time. Top row: no water accumulation (left), 4L water accumulation (right). Bottom row: 10L water accumulation (left), 20L water accumulation (right). The location of V-section is indicated by black dashed lines. From top to bottom, the dashed lines mark the V-section location for thin, flat, thick, and straight cables. Blue arrows indicate flow direction in each fiber section. Black arrow highlights the vibration of flat cable associated with the wavy liquid surface.

In further data analysis, each channel's spectrum was computed on a per-second basis, facilitating spectrum analysis with a specific emphasis on the V-section across various cable designs. This analytical approach produced a spectrum curve for each cable design at different water levels, as illustrated in Figure 9. Across all cable designs, a distinctive peak consistently emerged at a frequency of 20 Hz, aligning with scenarios of no water volume presence. However, as the volume of water increased, this 20 Hz peak gradually diminished, reflecting the dampening effect of water on vibration patterns.

Furthermore, our analysis involved the computation of standard deviation values for each second within every channel of the DAS data. By visualizing the data in this manner, we observed the onset of slug-like behavior at a velocity of 4 m/s with a water volume of 20L. The spectrum curve for 20L did not show similar trends to those of 10L, 4L and 0L (single

phase). This deviation in the 20L data can be attributed to the emergence of slug behavior, a phenomenon not observed at lower water volumes. Consequently, this behavior departs from the trends observed at 20 Hz.

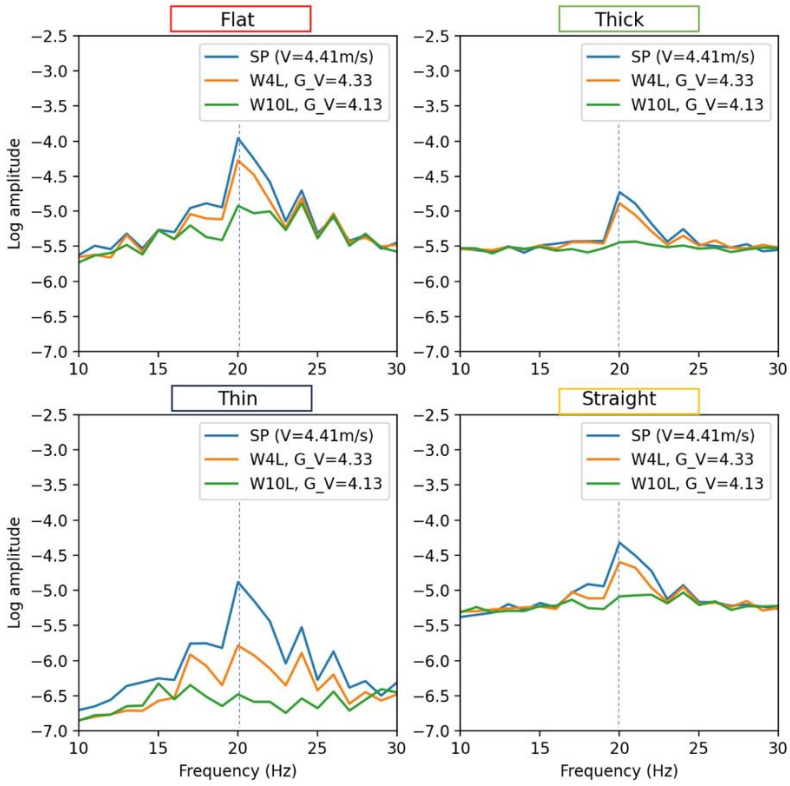

Figure 9. Frequency spectrum of DAS measurements near the V section for various cables at a gas velocity of approximately 4 m/s. SP (single phase) denotes conditions with no water accumulation. W4L, W10L, and W20L correspond to 4L, 10L, and 20L of accumulated water, respectively. Amplitudes are presented in a logarithmic scale. The prominent peak around 20 Hz is distinctly indicative of the accumulated water volume.

3.2. Task#2: Detection of Dynamic Intermittent (Slug) Structure

The experimental investigation of multiphase flow, where the water flow rate was consistently maintained at 0.6 GPM (superficial velocity at around 0.005m/s) while air flow rates were systematically adjusted to achieve velocities ranging from 18 m/s to 2 m/s, has yielded significant insights into the capability of DAS to capture dynamic intermittent slug structures. The DAS system demonstrated its capacity to effectively capture slug events. Figure 10 provides a visual representation of the raw DAS cable responses during slug and non-slug conditions, highlighting the system's sensitivity to slug detection. For improved visualization and analysis, standard-deviated processed data was employed, as exemplified in Figure 11. Processed DAS data exhibited a robust correlation with pressure sensor readings, with elevated values consistently corresponding to the presence of slugs at different time points (Figure 12).

To assess the sensitivity of different cable types, single traces for each cable design were analyzed and shown in Figure 13. The sensitivity analysis was further refined by comparing a single channel located near the pressure sensor for each cable type. This evaluation revealed that flat cables exhibited the highest sensitivity, followed by thin, straight, helical, and thick cables. Additionally, all channels corresponding to different cable types were averaged, as demonstrated in Figure 14. This approach offers the potential for the development of algorithms designed to detect slug occurrences using averaged standard deviation processed data. Observations indicated that slug frequency tended to increase as the gas flow rate reduced in the current experimental range. This can also be seen from Figures 11 and 12, where the white/red lines represent slugs. The denser lines indicate more slugs, i.e., a higher slug frequency.

These findings underscore the effectiveness of DAS in capturing dynamic slug structures within multiphase flow scenarios. The differential sensitivity of various cable types presents opportunities for tailored monitoring solutions, and the correlation between DAS data and pressure readings further validates its utility in real-time monitoring and detection applications. The observed trends in slug frequency with varying velocities may provide valuable insights for pipeline management and maintenance strategies.

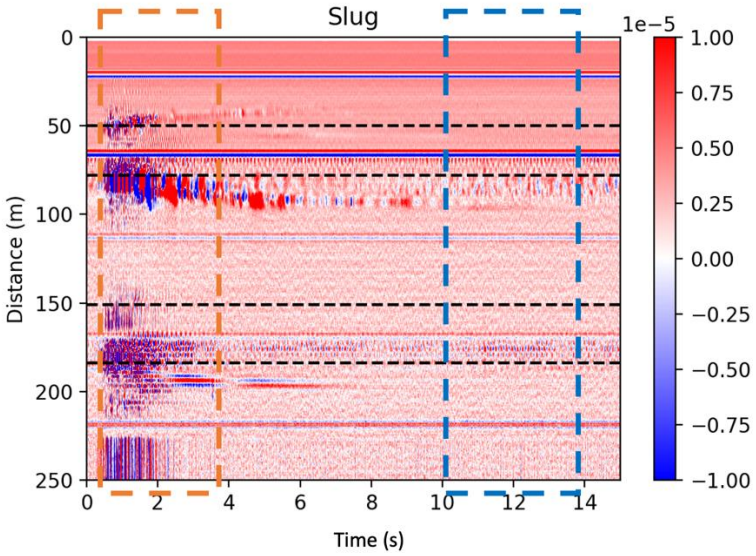

Figure 10. Raw DAS data at 6 m/s air flow velocity showing the slugging behavior captured on the thin, flat, thick, and straight cables, with the V location indicated by the black dashed line. The orange box encompasses the time when a slug is occurring, and the blue box encompasses the time when there is no slug.

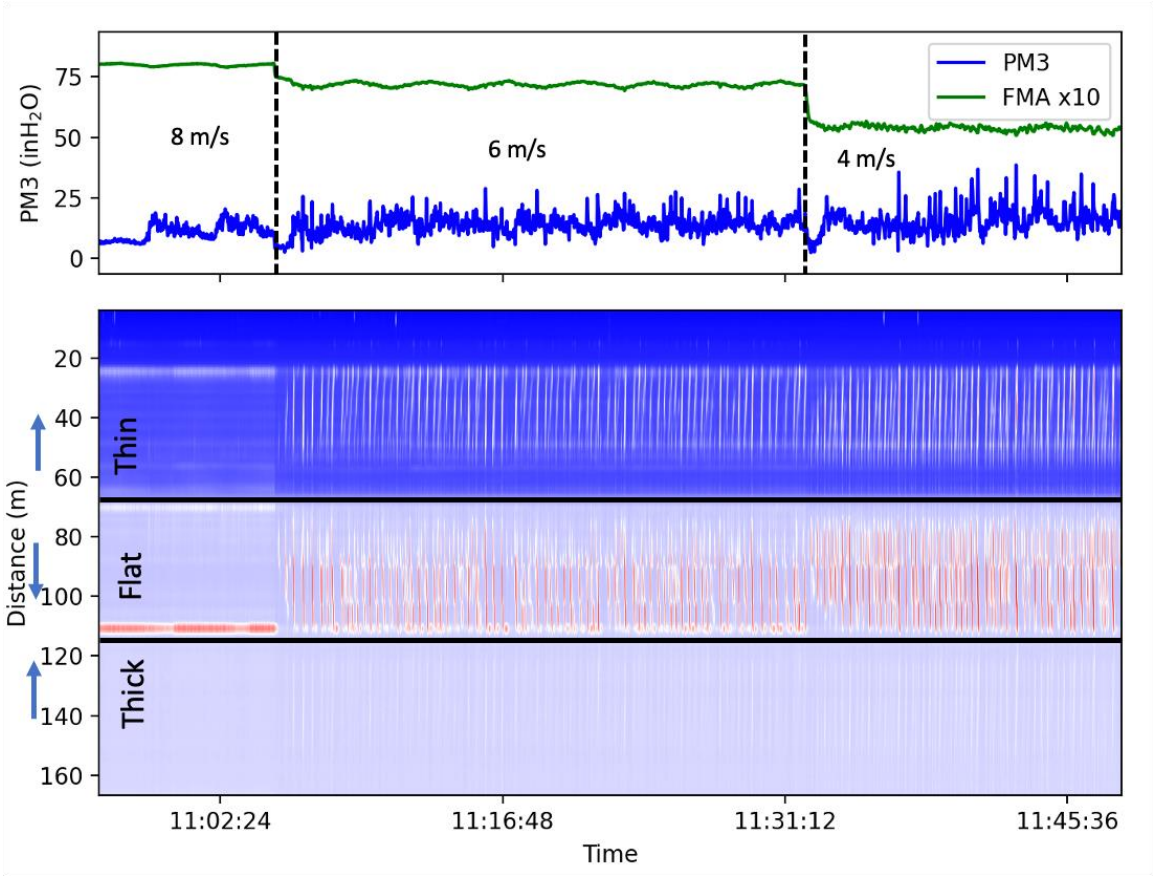

Figure 11. This waterfall plot includes the cable sections for the thin, flat, and thick cable designs, illustrating processed DAS data over time periods corresponding to velocities of 8 m/s, 6 m/s, and 4 m/s. The processed DAS data is presented alongside the uphill pressure sensor (PM3) and air flow rate (FMA). The water flow rate remained constant at 0.6 GPM; however, the air flow rate was adjusted to achieve the desired velocities. Slug phenomena can be observed at velocities of 6 m/s and 4 m/s. Stratified flow was observed at 8 m/s/

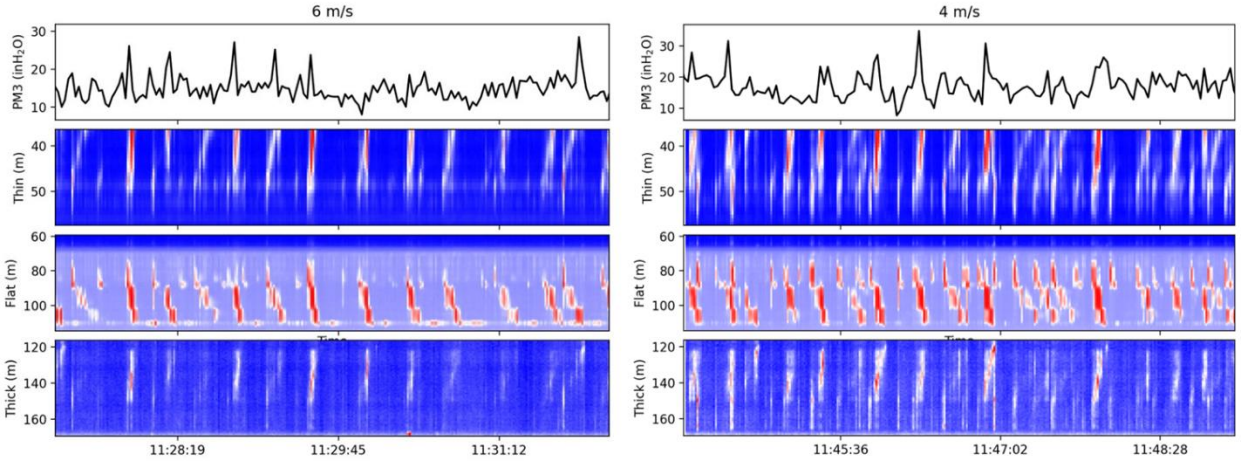

Figure 12. These waterfall plots include the cable sections for the thin, flat, and thick cable designs for different air flow rates (6 and 4 m/s). The top plots are the corresponding pressure measurement in the middle of the uphill section. Overall, the slug signal from DAS corresponds well with that from the pressure measurement.

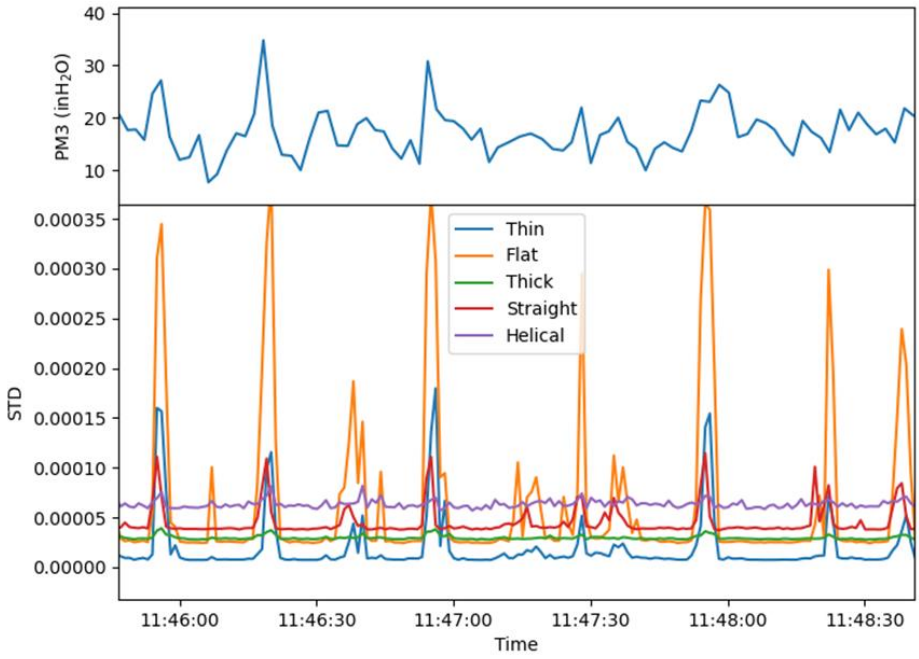

Figure 13. The bottom plot shows the single trace at location near uphill pressure sensor location for each cable design - thin, flat, thick, straight, and helical cables of processed DAS data. The top plot is the corresponding pressure measurement. Here, we can observe that the flat cable has the largest sensitivity to slug detection, followed by the thin, straight, helical, and thick cables.

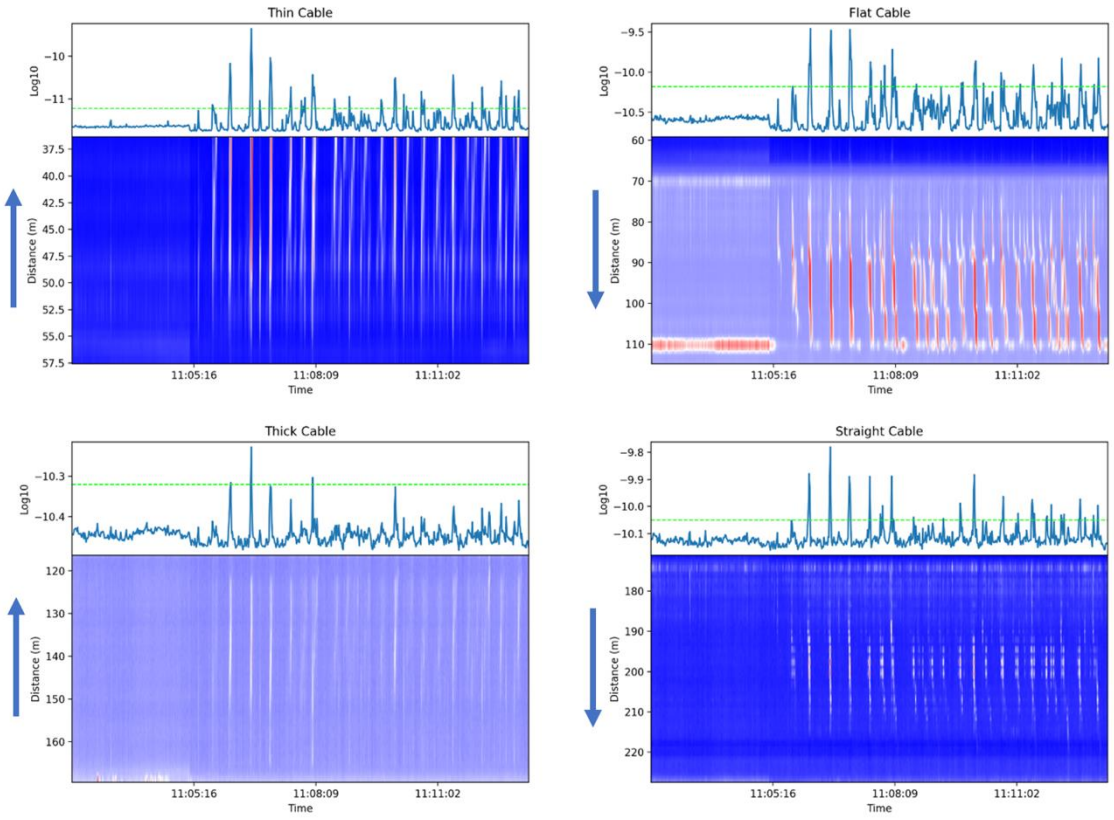

Figure 14. Waterfall plots of processed DAS data, standard deviation DAS data for every second per channel, for the thin, flat, thick, and straight cable designs. Top plots on top of waterfall plots show the average standard deviation of the channels that correspond to the different cable designs. The high standard deviation log-scaled values correspond with slugs observed in the multiphase flow.

3.3. Task#3: Detection of Corroded Spots on Pipeline Interior Surface

For this task, we have completed the experiments using the 1-m test section with a 3 mm corrosion depth at 6'Oclock position, at sparsely supported condition (5 supports). Preliminary data analysis, however, has shown only slight variations between the baseline (no corrosion) and measurements taken at a corrosion depth of 3 mm.

Figure 15 provides a visual representation of 0.2 seconds' worth of raw DAS data, illustrating examples from black and flat cable sections.

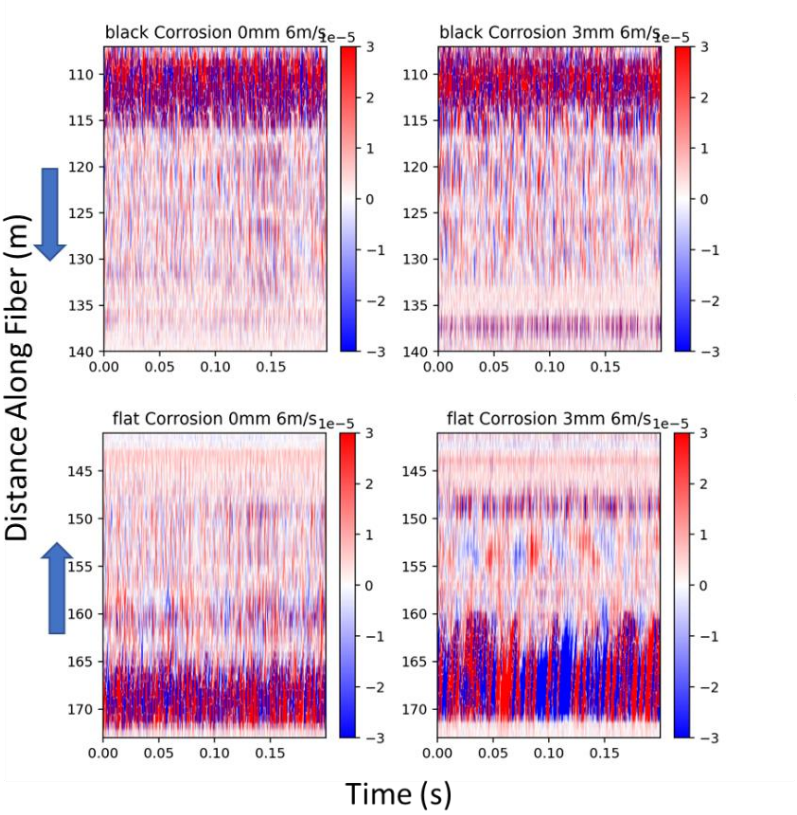

Figure 15. Examples of raw DAS data waveforms from black and flat fiber sections for Task#3. Left column shows the baseline without corrosion, and right column shows measurements with the pipe with 3-mm corroded depth. Blue arrow shows the gas flow direction in the fiber sections.

For a more quantitative comparison, we calculated the average vibration amplitude over an eight-minute period within the frequency range of 100 Hz to 1000 Hz. This amplitude, plotted against fiber distance, is depicted in Figure 16. The measurements were taken at a velocity of 6 m/s, and similar results were obtained at other velocities.

Our results demonstrate that, even after a complete reinstallation of the flow loop to replace a 1-m section in the middle, the DAS measurements within each section are remarkably consistent. This consistency testifies to the repeatability of our experimental setup.

Since 3 mm represents the minimum designed corrosion depth, it's plausible that the internal cables may not be sensitive enough to detect such minor corrosions. In the future, we will enhance our data analysis methods to more effectively extract useful data attributes for corrosion detection. Simultaneously, we prepared another 1-m test section with a more severe corrosion depth. The corrosion eventually resulted in a tiny leakage at the pipe bottom with a size of 2 mm approximately (Figure 17). We are preparing the 3rd 1-m test section with a corrosion depth at around 5.5 mm that simulates the severe corrosion scenario before leakage happens. We are planning to conduct the experiments using these two new test sections next quarter.

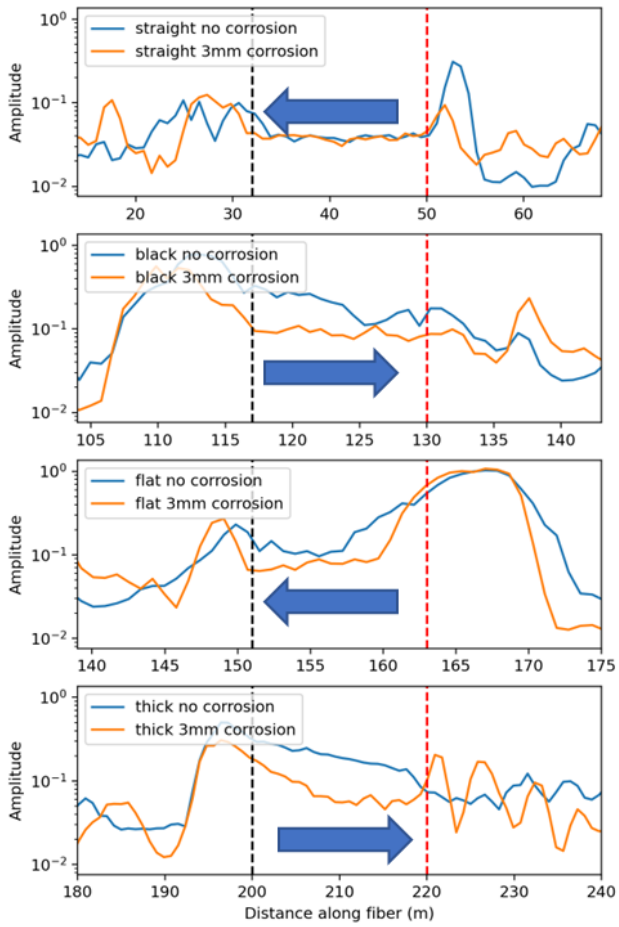

Figure 16. Vibration amplitude comparison at different fiber sections (straight, black, flat, and thick) between the corroded pipe and the baseline. These measurements were taken with a gas flow velocity of 6 m/s, and the data were filtered between 100 Hz and 1000 Hz. The arrow shows the flow direction compared to the fiber distance. Black and red dash lines mark the beginning and end of each section.

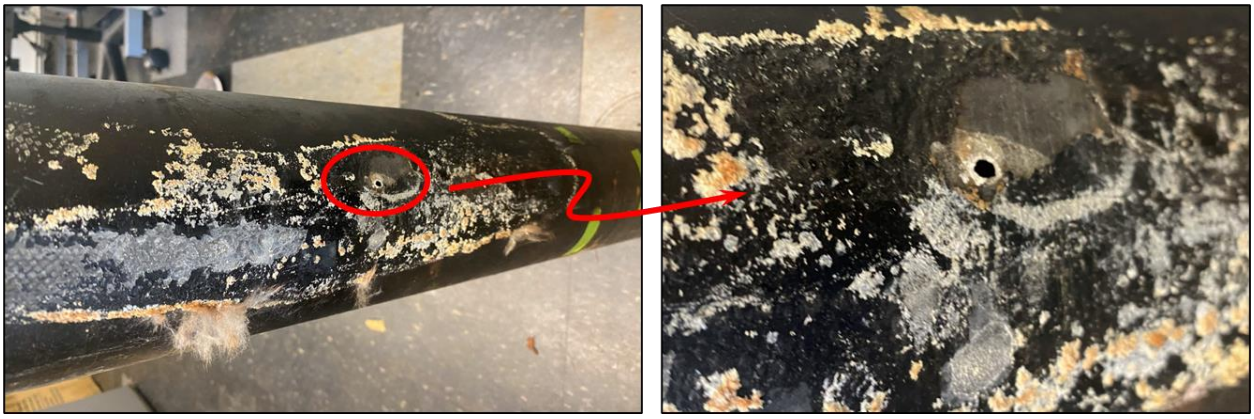

Figure 17. Photograph of the pipe bottom with breakthrough spot

3.4. Task#4: Detection of Dent/Deformation on Pipeline

During the past year, we worked with EMI (the Excavation Engineering and Earth Mechanics Institute) at the Colorado School of Mines on the fabrication of dents in the 1-m test section. We have successfully prepared two deformed pipes with different dent sizes. The pipe that exhibits a substantial deformation represents a significant structural compromise, while the other that showcases a smaller dent simulates a less severe scenario, as depicted in Figure 18. Our intention is to test these two differently deformed pipes in the flow loop during the upcoming reporting period.

Figure 18. Photograph of the facility that created the dents and the 1-m test sections with two dent sizes.

3.5. Task#5: Detection of Infrastructure Damage

During the past year, we finished experiments for infrastructure damage under densely and sparsely supported conditions. In the sparsely supported condition, 5 supports were distributed evenly along the 21m steel pipeline in the base case. The second support from the inlet was removed to simulate the scenario of support damage, resulting in a total of 4 supports for the damaged support condition. In densely supported conditions, 6 supports were used in the base case, and the same support was removed to simulate the support damage.

Every infrastructure possesses its own unique resonant frequencies, which are determined by the structure's elastic properties and various boundary conditions such as support, surrounding materials, and more. For our task, the removal of one support from the pipeline is likely to alter the boundary conditions of the structure. This alteration could provoke changes in both the frequency and amplitude of the structure's resonant vibration modes.

To extract these resonant frequencies, we carried out spectrum analysis using the Fourier transform. The collected DAS data were divided into 10-second sections, with a Fourier transform performed on each channel. We then averaged the spectra over eight-minute intervals during each experiment. The resulting amplitude spectrum for the sparsely supported condition, when plotted against the fiber distance, can be seen in Figure 19.

As shown in Figure 19, the steel pipe vibrates at discrete resonant frequencies with an interval of approximately 120 Hz as the gas flows. These are illustrated by the vertical line-like patterns in the colormap plots. Each resonant frequency, characterized by alternating sections of higher and lower amplitude along the pipe, can be effectively explained by the theory of standing waves. For a standalone pipeline, the frequency and amplitude of each resonant mode, especially the higher frequency ones, are closely associated with the boundary condition of the pipe. In this experiment, we altered the boundary condition by removing one of the weight-bearing supports of the steel pipe, which in turn changed the resonant vibration patterns. A comparison of the left and right subplots in Figure 19 reveals that the vibration pattern is fairly consistent between the two cases. However, a detailed analysis shows that the frequency and amplitude of several resonant modes have changed after reducing the number of supports from five to four. As shown in Figure 20, the resonant mode at around 700 Hz exhibits two adjacent frequency peaks. After the removal of the support, these two frequency peaks merged into one. We also observed a slight frequency shift in several vibration modes. For instance, the peak at 583 Hz shifted to 585 Hz following the removal of the support. Similar results can be seen in the densely supported experiments.

All cables are able to detect these changes at a gas rate of 6 m/s, although the noise floor of the internal cables (black, flat, and thick) is higher than that of the external one (straight), likely due to flow-cable interaction. Owing to its geometry, the flat cable demonstrates the highest noise level in this case. The frequency spectrum from the flat cable also reveals minor frequency peaks, probably linked to the flow-induced cable resonant vibration.

At a higher gas rate, the signal-to-noise levels of the internal cables are further reduced. Nevertheless, we can still identify the frequency changes of resonant modes in the internal cables at the highest gas rate (18 m/s). However, at the lowest gas rate (2 m/s), very little pipe vibration can be detected by any of the cables, rendering the measurements unsuitable for identifying infrastructure damage.

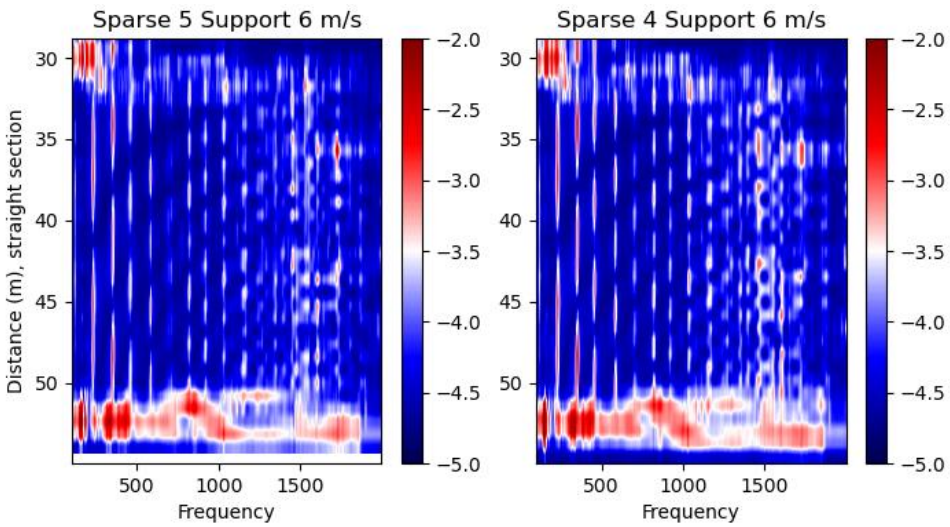

Figure 19. Frequency Spectrum of the straight fiber section with gas flow rate at 6 m/s. Vertical axis is the distance along the fiber/pipe, horizontal axis is frequency. Warmer color indicates higher amplitude at a certain frequency/location. The color is in log scale.

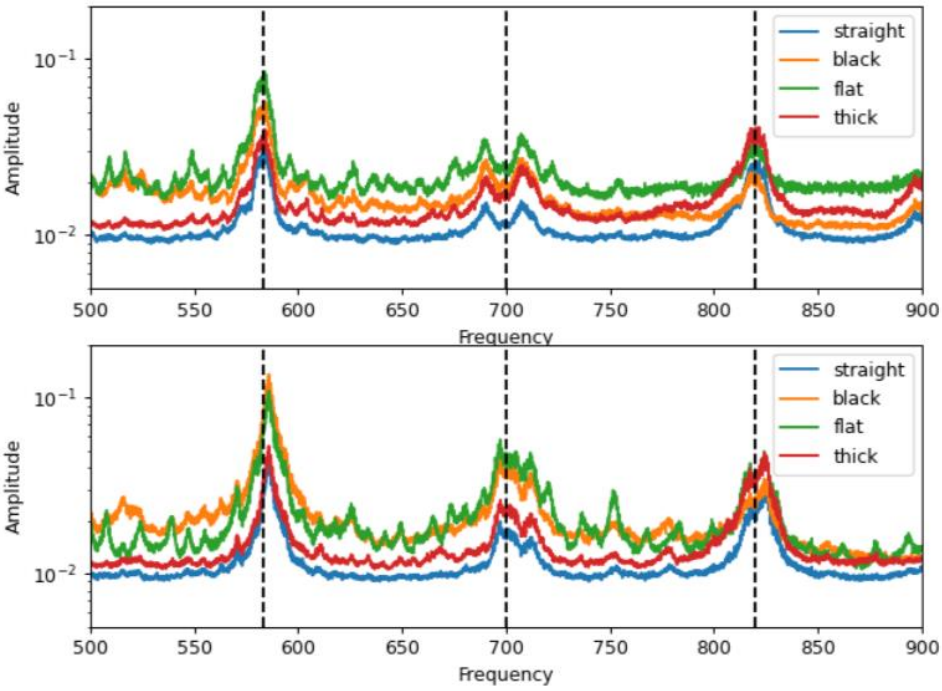

Figure 20. Averaged frequency spectrum of each fiber section zoomed in between 500 Hz and 900 Hz. Top panel shows measurements with 5 supports, while the bottom panel shows those with 4 supports that simulates a scenario with a damaged support. Dashed line marked the estimated resonant frequency of three vibration modes.

3.6. Task#6: Detection of Leakage

During the past period, we conducted the leakage tests using a 1-m test section with 1-in. holes at three different positions to simulate the leakage at different orientations. With reducers, we were able to test four leakage sizes, namely ¼", ½", ¾", and 1". Five gas flow rates, 2, 6, 10, 14, 18 m/s, were tested. We also did the experiments at the same flow rate without any leakage, which is referred to as the controlled tests in the following data analysis.

During this task, the DAS data were recorded at a frequency of approximately 5600 Hz along a 480-meter fiber, generating a substantial volume of data in a short period. For instance, the three-hour recording session yielded over 150 GB of DAS data. Due to its size, this data set requires pre-processing before any meaningful analysis can be conducted. The first processing we conducted was based on the standard deviation (STD). We segment the data set into one-second intervals and compute the STD for each channel within each second. These STD values are then concatenated into a continuous data set with a 1 Hz sampling rate. This method allows for a data reduction factor of 5600, equivalent to the original sampling rate. Figure 21 provides an illustrative example of the STD data attributes during an experiment involving bottom leakage holes. In this figure, a higher value (depicted in red) signifies a larger standard deviation at a specific time and location along the sensing fiber, which in turn is indicative of higher vibration intensity experienced by the cable section.

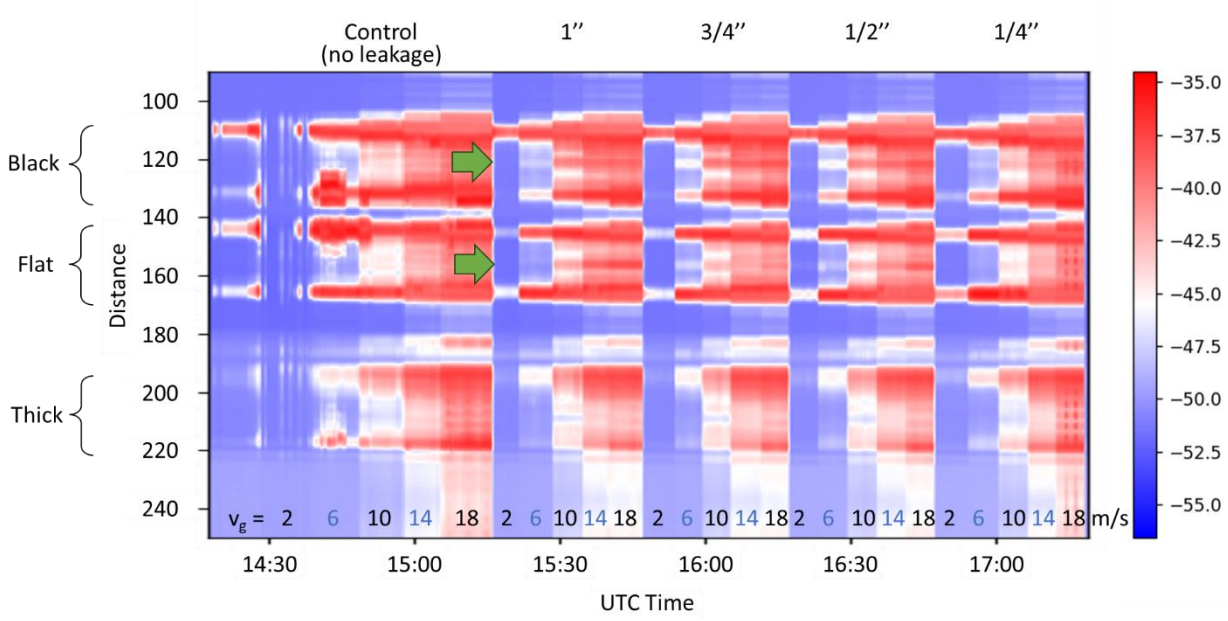

Figure 21: Magnitude of standard deviation values along the fiber during the experiment on August 17th, 2023. For each hole size, the flow rate changes from 2, 6, 10, 14 and 18 m/s. The gas velocities are indicated at the bottom of the image.

The figure displays the vibration intensity for three distinct types of cables during the experiment conducted on the same day. The study commenced with a control experiment featuring no leakage, followed by the sequential introduction of 1", ¾", ½", and ¼" leakage

holes at the bottom of the test pipe. For each hole size, flow rates of 2, 6, 10, 14, and 18 m/s were examined. Figure 21 clearly reveals variations in fiber vibration intensity at different flow rates, with higher flow rates inducing stronger vibrations across all cable types.

Notably, more intense vibrations are visible near the pipe's center, where the leakage was introduced, for both black and flat cables. The vibration anomaly appears to diminish with decreasing hole size and is entirely absent in the control tests.

To quantify the vibration anomalies associated with the leakage points, we calculated the average vibration intensity over a four-minute span in the middle of each experiment. This average intensity forms a vibration profile for each cable, and the amplitude is then converted to decibels (dB) for easier comparison.

Figure 22 showcases the sensitivity of different cables to varying leakage sizes. At a flow rate of 10 m/s, all three cable types can detect a vibration anomaly when the leakage hole is larger than ½".

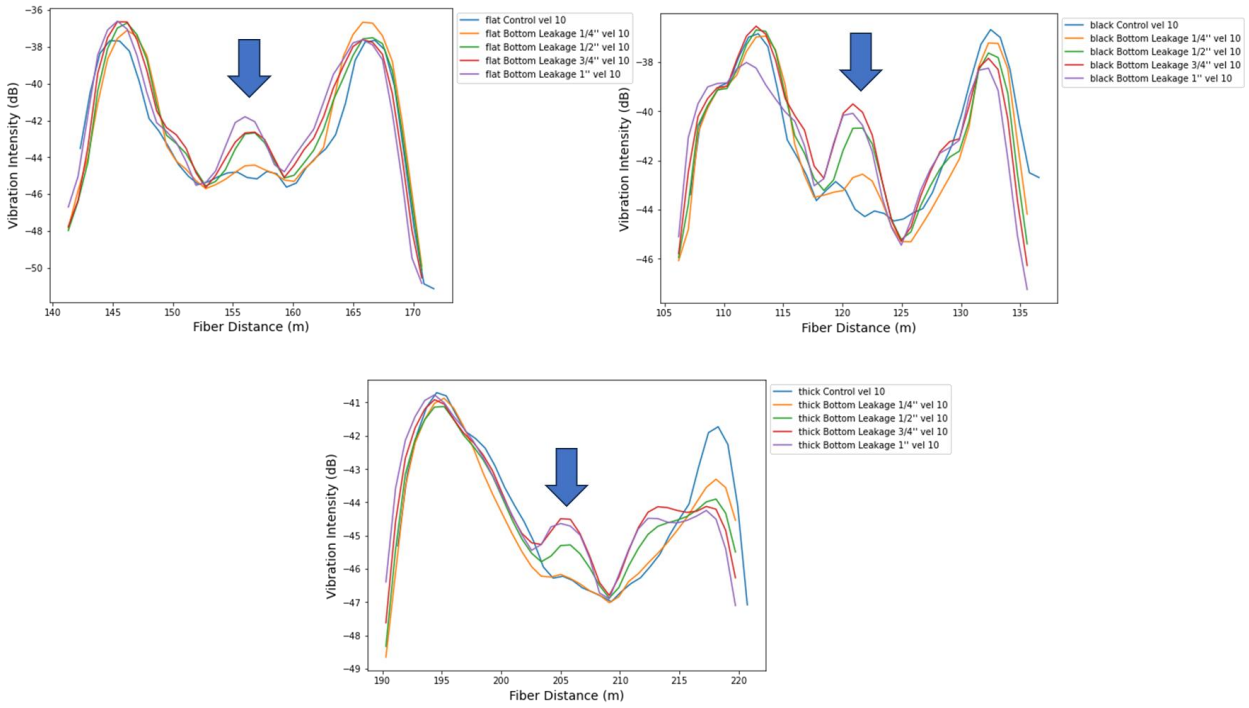

Figure 22: vibration intensity profiles in flat (upper left), black (upper right), and thick (bottom) fiber sections during the leakage experiment. The different curves represent vibration intensities associated with varying leakage hole sizes at a flow rate of 10 m/s. Anomalies in vibration, induced by leakage holes and marked by blue arrows, are observable in all three cable types when the hole size exceeds 1/2 inch.

Leakage detection sensitivity is also influenced by the gas flow rate within the pipe. Figure 23 illustrates the vibration distribution along each internal fiber cable at different flow rates. For instance, in the control experiment, vibration intensity escalates with increasing flow rates for the flat cable, and no vibration anomaly is observable at the pipe's center.

Conversely, in the experiment with a ½" leakage hole, a vibration anomaly is observable at all flow rates for both flat and black cables, whereas for the thick cable, the anomaly is only evident at 10 m/s.

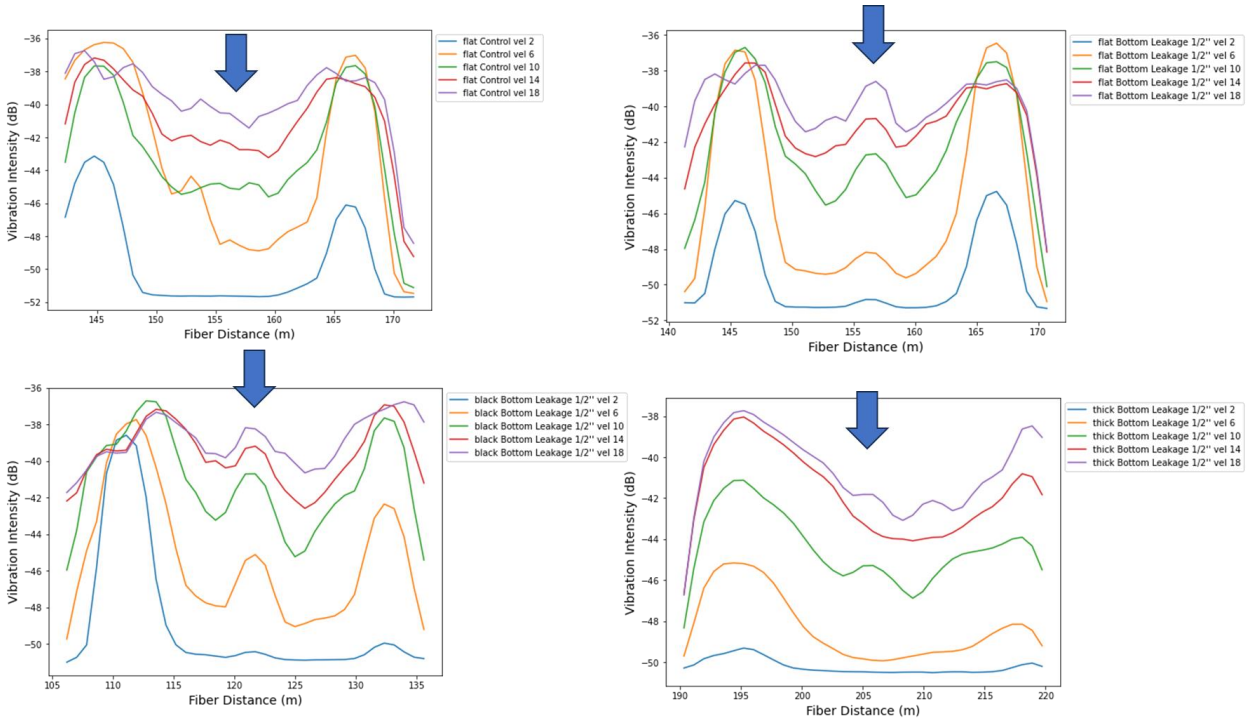

Figure 23: This figure compares the leakage detection sensitivity across different cable types at varying flow velocities. Top left shows a flat cable without leakage as a control experiment. Top right features a flat cable with a leakage hole size of 1/2 inch. The bottom left and bottom right sections present the black cable and thick cable with the same leakage size, respectively.

Our findings suggest that black and flat cables offer the most reliable leakage detection results to date. Their lighter and more flexible structures likely render them more sensitive to fluid movements within the pipe.

Lastly, it should be noted that we were unable to achieve satisfactory detection results with external cables, likely due to poor mechanical coupling between the cable and the steel pipe.

To better understand the cable vibrations induced by leakage, we conducted a Fourier spectrum analysis on the DAS measurements. The primary objective of this analysis is to identify the frequency range associated with the leakage-related signals. Acquiring this information will aid in optimizing leakage detection algorithms and refining future data acquisition parameters.

In our analysis, raw DAS data were segmented into 10-second intervals, and the amplitude spectrum was computed for each channel. To improve statistical reliability, spectra obtained from 4-minute measurements during the same experiments were stacked and averaged. The resulting spectra are organized as 2D arrays, where each column represents the spectrum

amplitude for a specific frequency and each row corresponds to the amplitude spectrum for an individual channel.

Figure 24 illustrates the 2-D spectra obtained from experiments involving various leakage sizes at the bottom of a pipe with a flow rate of 10 m/s. High amplitude spectra are conspicuously evident near the leakage points (indicated by blue arrows in Figure 24) for most cases involving black and flat cables. However, the leakage point is less identifiable in the spectra of thicker cables.

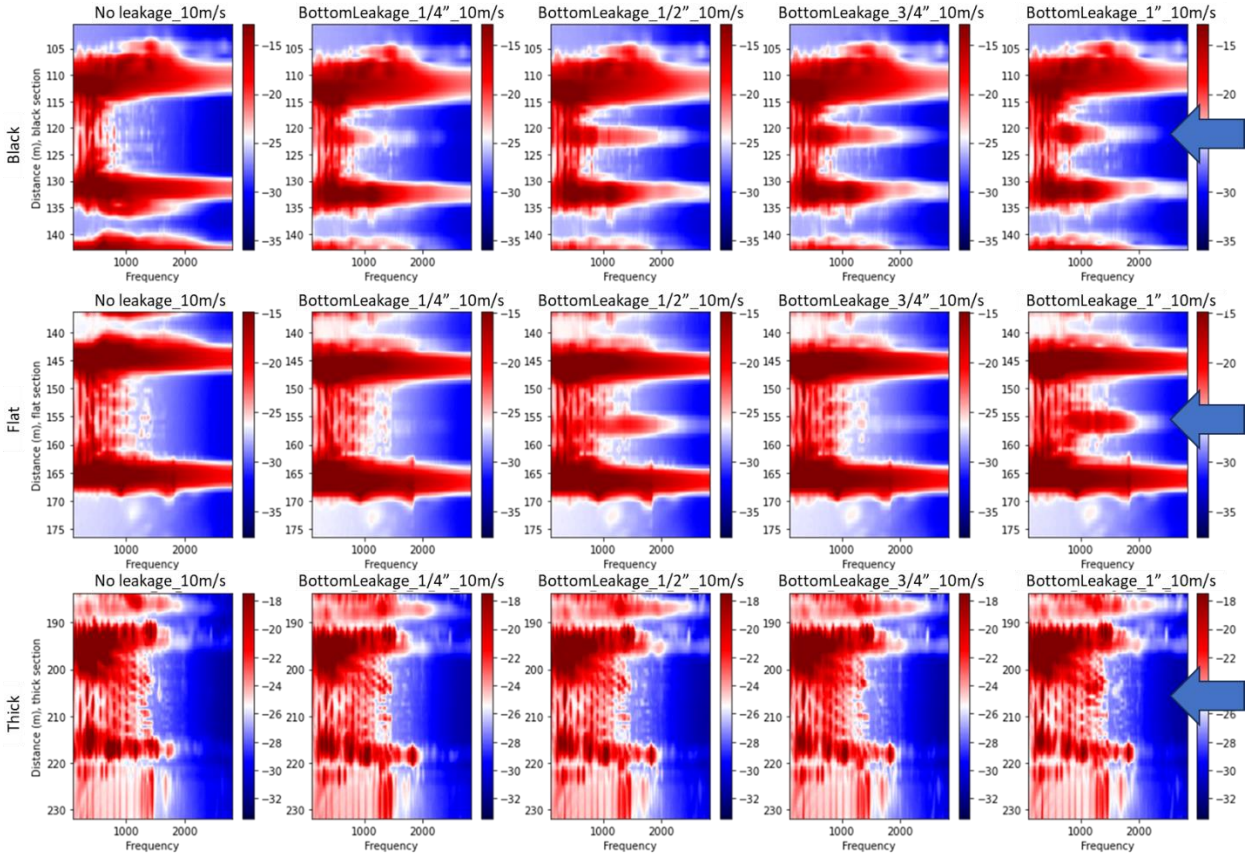

Figure 24: 2D spectra of fiber sections with varying leakage hole sizes at the bottom of the pipe, measured at a flow rate of 10 m/s. The top row displays the black cable section, the middle row showcases the flat cable section, and the bottom row features the thick cable section. Columns from left to right represent the control experiment (no leakage), followed by leakage sizes of ¼", ½", ¾", and 1", respectively. The color scale is measured in dB. Blue arrows show the leakage point location.

To visualize the amplitude spectrum induced by the leakage more clearly, we extracted the amplitude values corresponding to the leakage location from the 2D spectra and plotted them against frequency. Figure 25 presents the amplitude spectrum for experiments with different leakage sizes, all at a flow rate of 10 m/s. The right column of Figure 25 shows the amplitude ratio between the leakage and control (no leakage) experiments. Our findings indicate that the vibrational anomalies caused by leakage span a broad spectrum. For black cables, we

observed up to a 10 dB increase in amplitude across most of the measured frequency range at the leakage point compared to the no-leakage scenario.

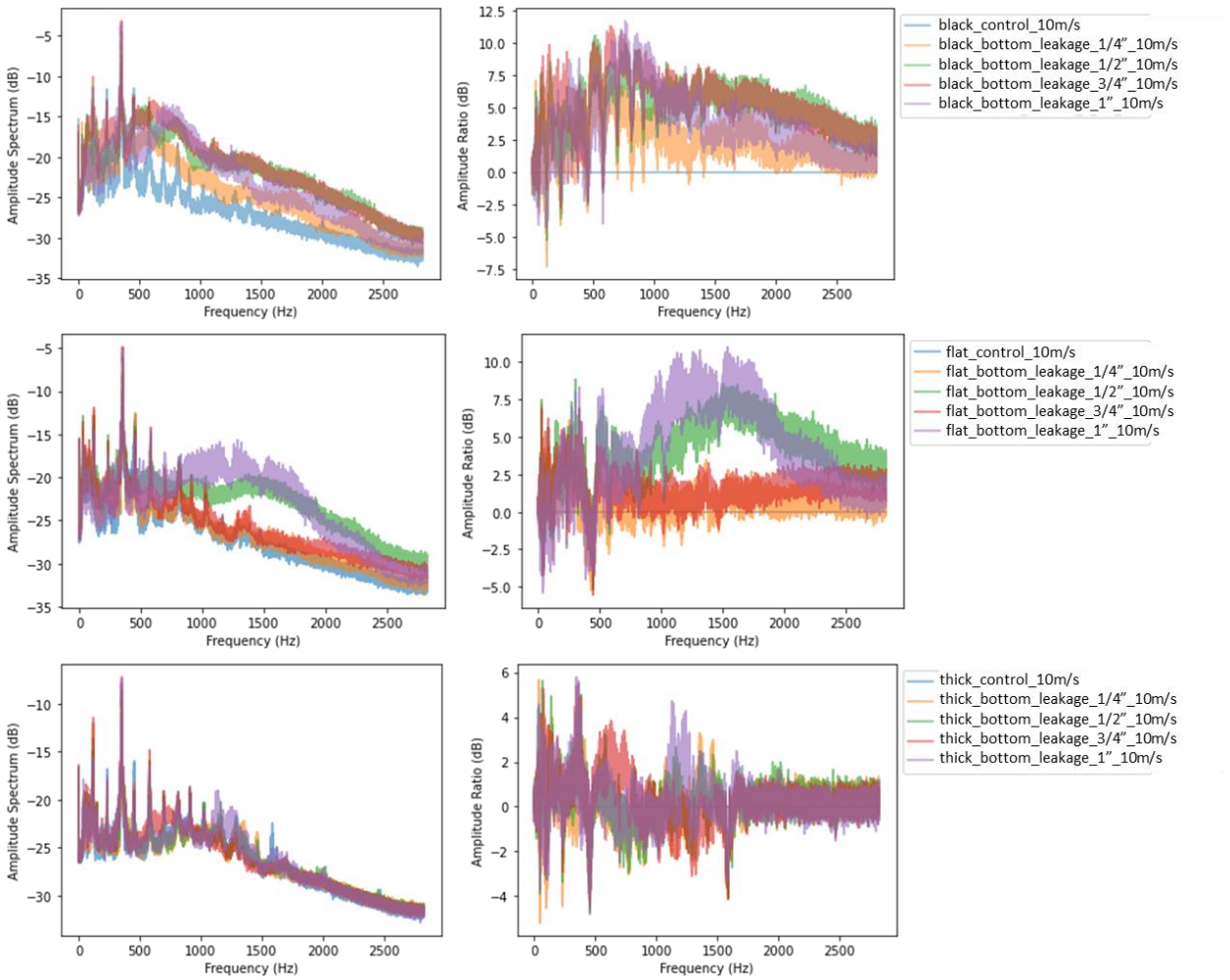

Figure 25: Amplitude spectrum at leakage point locations for various cables and leakage sizes. The flow rate is 10 m/s. The first row displays results for black cables, the second row for flat cables, and the third row for thick cables. The left column shows the amplitude spectrum, while the right column presents the ratio of amplitude spectrum between leakage experiments and the control experiment. All values are expressed in decibels (dB).

The spectral responses appear to be more complex for flat cables. For instance, with leakage sizes of ¼" and ¾", amplitude increases are more uniformly distributed across the entire frequency band, averaging between 1-2 dB. Conversely, for ½" and 1" leakage sizes, the amplitude increases are predominantly concentrated in the 1000-2000 Hz range, exceeding an average of 5 dB. This complex response to leakage is likely due to the flow interactions between the flat cable and the flow deviating from the main pipe into the leakage pathway. In contrast, little amplitude increase can be observed on the thick cable, which is consistent with the STD results. At large leakage sizes, amplitude increase can be observed at a narrower frequency band, with 600-800 Hz for the ¾'' leakage size and 1100-1300 Hz for 1" leakage

size. Further analyses are underway to understand these physical phenomena better.

From the results, we found that the black cable seems to provide more reliable differentiation between leakage and control experiments, which could potentially lead to more reliable leakage detection.

The same analysis was carried out for experiments in which leakage points were introduced at the top and side of the steel pipe. Because these experiments were conducted on different dates from the control experiment, the DAS instrument was disconnected and then re-spliced to the sensing fiber. This action led to a change in the measurement noise floor. Figure 26 presents a comparison of vibration intensity and spectrum analysis for the black cable in both the side and top leakage experiments, conducted at a flow rate of 10 m/s.

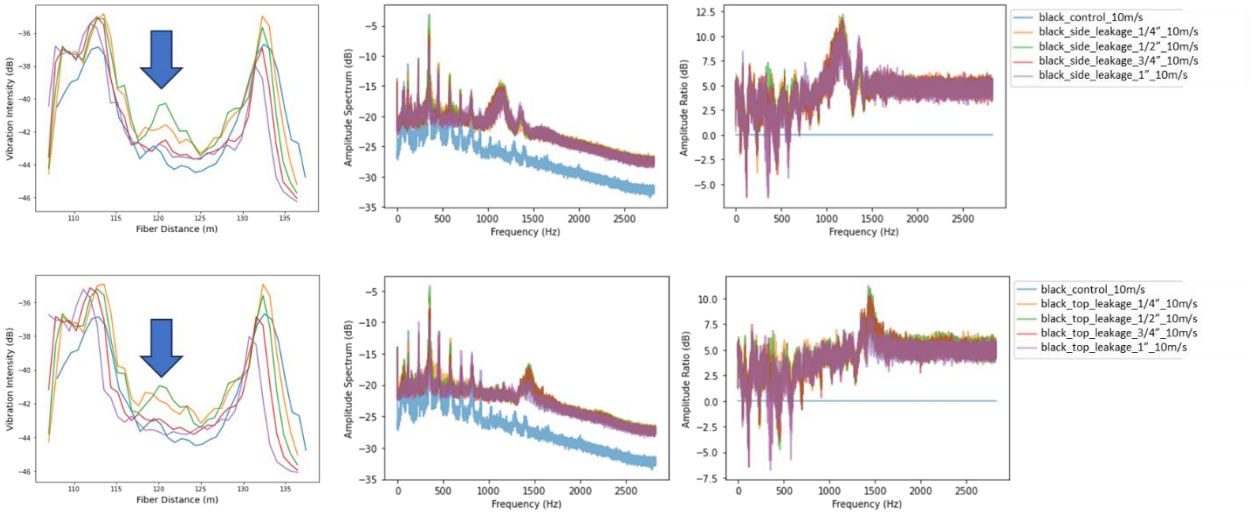

Figure 26: Results from experiments with the black cable where leakage points were introduced at the side and top of the pipe. Top row: side leakage experiments. Bottom row: top leakage experiments. Left column: vibration intensity profiles with varying leakage sizes. Middle column: amplitude spectra at the leakage points. Right column: amplitude ratio between the leakage experiments and the control experiment. The leakage experiments were conducted on different dates than the control experiment, and the fiber was respliced between experiments.

We observed that, based on the vibration intensity, spatial identification of the vibration anomaly becomes more challenging for the top and side leakage experiments. Stronger anomalies seem to be associated with smaller leakage sizes, but this trend was not observed at other flow rates or with other cables. The amplitude spectrum results revealed variations in noise levels, which are likely due to the re-splicing of the fiber. Increased amplitude was noted around 1200 Hz for side leakage and 1500 Hz for top leakage. At this stage, it is unclear whether these amplitude increases were induced by the leakage itself.

To improve the reliability of our findings, we plan to redo the top and side experiments, and repeat the control experiment prior to each leakage experiment for more consistent comparison. This approach will help us better identify signal changes specifically attributable to the leakage.

4. Future work

In the next quarter, we plan to 1) complete Task#2 by finishing another water flow rate at around 0.0025 m/s and exploring deeper the corresponding data analysis; 2) complete the steel pipe experiments (Tasks#3-6) in supported conditions and perform corresponding data processing. In 2024, we will start experiments for unburied and buried pipes.

References

1. PHMSA: Stakeholder communications - smart pig fact sheet. https://primis.phmsa.dot.gov/comm/FactSheets/FSSmartPig.htm?nocache=4003.
2. Zhang, S., Liu, B. & He, J. Pipeline deformation monitoring using distributed fiber optical sensor. *Measurement (Lond.)* **133**, 208–213 (2019).
3. Inaudi, D. & Glisic, B. Long-range pipeline monitoring by distributed fiber optic sensing. *J. Press. Vessel Technol.* **132**, 011701 (2010).
4. Muggleton, J. M., Hunt, R., Rustighi, E., Lees, G. & Pearce, A. Gas pipeline leak noise measurements using optical fibre distributed acoustic sensing. *Journal of Natural Gas Science and Engineering* **78**, 103293 (2020).
5. Nikles, M. *et al.* Leakage detection using fiber optics distributed temperature monitoring. *Smart Structures and Materials 2004: Smart Sensor Technology and Measurement Systems* Preprint at https://doi.org/10.1117/12.540270 (2004).
6. Grosswig, S., Hurtig, E., Luebbecke, S. & Vogel, B. Pipeline leakage detection using distributed fibre optical temperature sensing. *17th International Conference on Optical Fibre Sensors* Preprint at https://doi.org/10.1117/12.623803 (2005).
7. Ukil, A., Libo, W. & Ai, G. Leak detection in natural gas distribution pipeline using distributed temperature sensing. *IECON 2016 - 42nd Annual Conference of the IEEE Industrial Electronics Society* Preprint at https://doi.org/10.1109/iecon.2016.7793562 (2016).
8. Jiang, T., Ren, L., Jia, Z.-G., Li, D.-S. & Li, H.-N. Pipeline internal corrosion monitoring based on distributed strain measurement technique. *Struct. Contr. Health Monit.* **24**, e2016 (2017).
9. Ravet, F., Niklès, M. & Rochat, E. A Decade of Pipeline Geotechnical Monitoring Using Distributed Fiber Optic Monitoring Technology. in *ASME 2017 International Pipeline Geotechnical Conference* (American Society of Mechanical Engineers Digital Collection, 2017). doi:10.1115/IPG2017-2503.
10. Tejedor, J. *et al.* A Novel Fiber Optic Based Surveillance System for Prevention of Pipeline Integrity Threats. *Sensors* **17**, (2017).
11. Stajanca, P. *et al.* Detection of Leak-Induced Pipeline Vibrations Using Fiber-Optic Distributed Acoustic Sensing. *Sensors* **18**, (2018).
12. Blevins, R. D. *Flow-induced vibration*. (1977).
13. Sarpkaya, T. *Vortex-Induced Oscillations A Selective Review*. http://www.asme.org/about-asme/terms-of-use (1979).
14. Yang, B., Gao, F.-P., Jeng, D.-S. & Wu, Y.-X. Experimental study of vortex-induced vibrations of a pipeline near an erodible sandy seabed. *Ocean Eng.* **35**, 301–309 (2008).
15. Naudascher, E. & Rockwell, D. *Flow-Induced Vibrations: An Engineering Guide*. (Courier Corporation, 2012).